Supporting Information

Leather-based flexible self-powered humidity sensors for respiratory monitoring

Jiansheng Wu[1], Hong Xie[1], Zhen Liu[1], Yitong Fu[1], Fenghui Yang[1], Le Chen[1], Wei Cheng[2], Bing Zheng[1]*, Fengwei Huo[1]*

1 Key Laboratory of Flexible Electronics (KLOFE) & Flexible Electronics (Future Technologies) & Institute of Advanced Materials (IAM), Nanjing Tech University, 30 South Puzhu Road, Nanjing 211816, China

2 Department of Dental Implantology, Nanjing Stomatological Hospital, Affiliated Hospital of Medical School, Institute of Stomatology, Nanjing University, Nanjing, China

*** Corresponding author**

Dr. Bing Zheng

Postal address: 30 South Puzhu Road, Nanjing 211816, China

Tel: + 86 025 83587982; E-mail address: iambzheng@njtech.edu.cn

Prof. Fengwei Huo

Postal address: 30 South Puzhu Road, Nanjing 211816, China

Tel: + 86 025 83587982; E-mail address: iamfwhuo@njtech.edu.cn

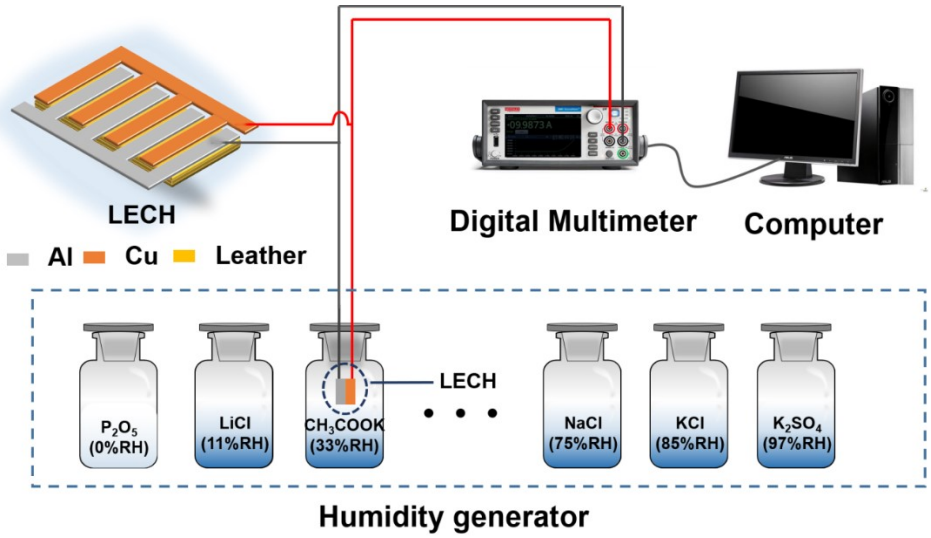

Fig. S1. Schematic diagram of the test system for the LECH sensor, where saturated solutions of P_2O_5, LiCl, CH_3COOK, $MgCl_2$, K_2CO_3, $Mg(NO_3)_2$, NaCl, KCl, and K_2SO_4 were obtained at 0%, 11%, 23%, 33%, 43%, 52%, 75%, 85%, and 97% relative humidity, respectively, in a closed wide-mouth bottle at 25°C.

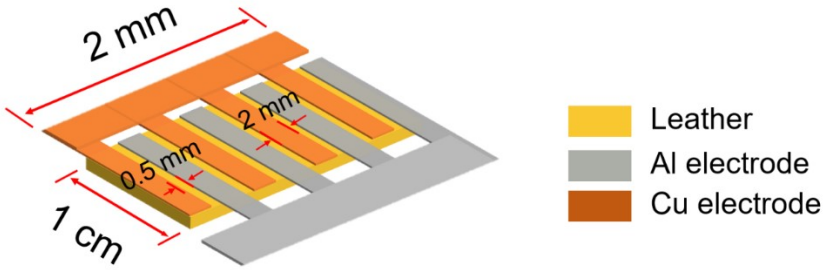

Fig. S2. Schematic diagram of the overall structural dimensions of the LECH sensor.

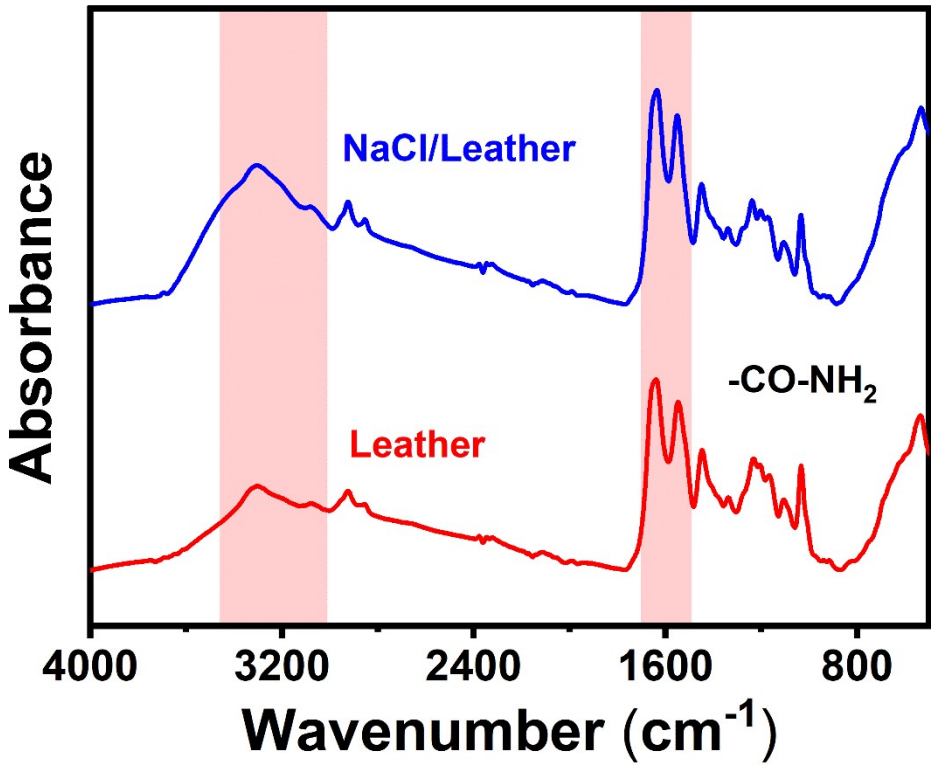

Fig. S3. FTIR spectra of pure leather and NaCl/leather.

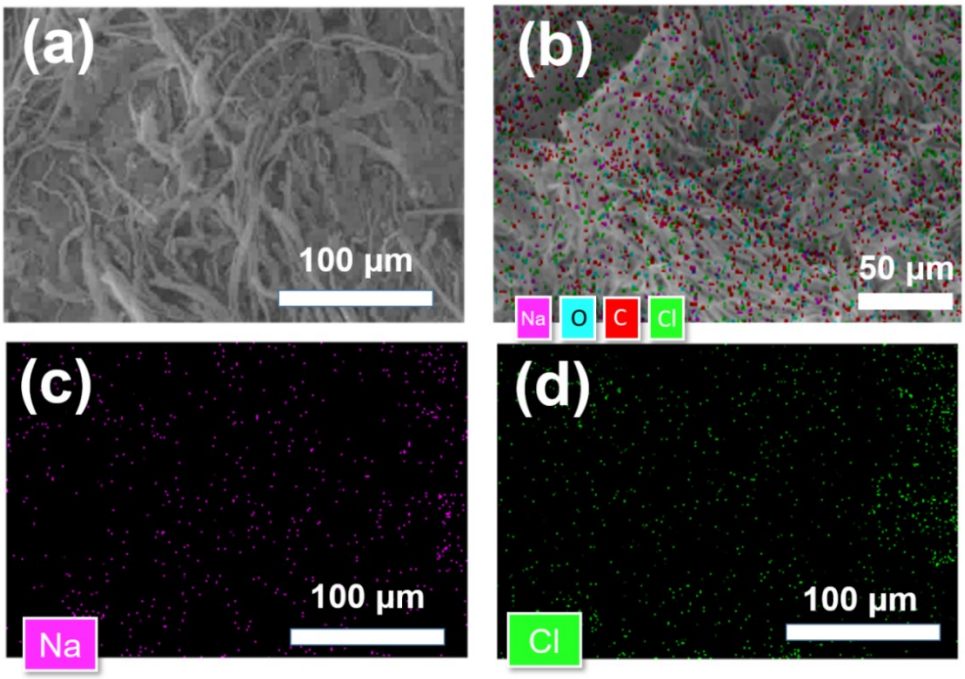

Fig. S4. The leather soaking in 2.5 mol/L NaCl solution. (a) SEM image (b) EDS mapping of the selected area, and (c–d) corresponding EDS mappings element of Na and Cl.

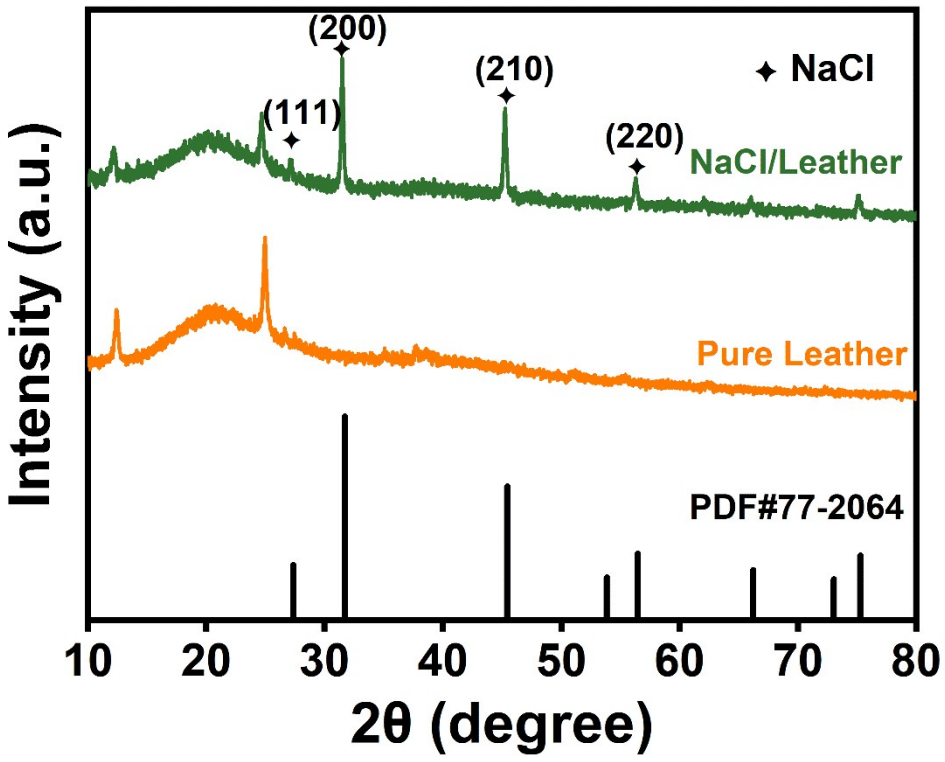

Fig. S5. XRD pattern of pure leather and NaCl/leather.

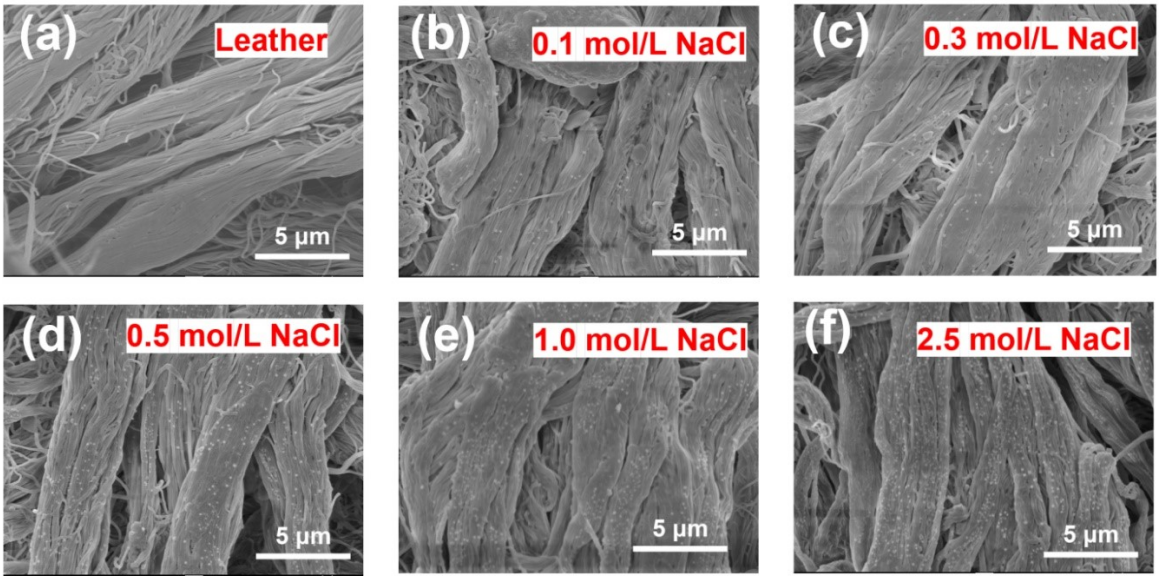

Fig. S6. SEM images of (a) pure leather, (b–e) leather soaked with 0.1 mol/L, 0.3 mol/L, 0.5 mol/L, 1.0 mol/L, and 2.5 mol/L NaCl , respectively.

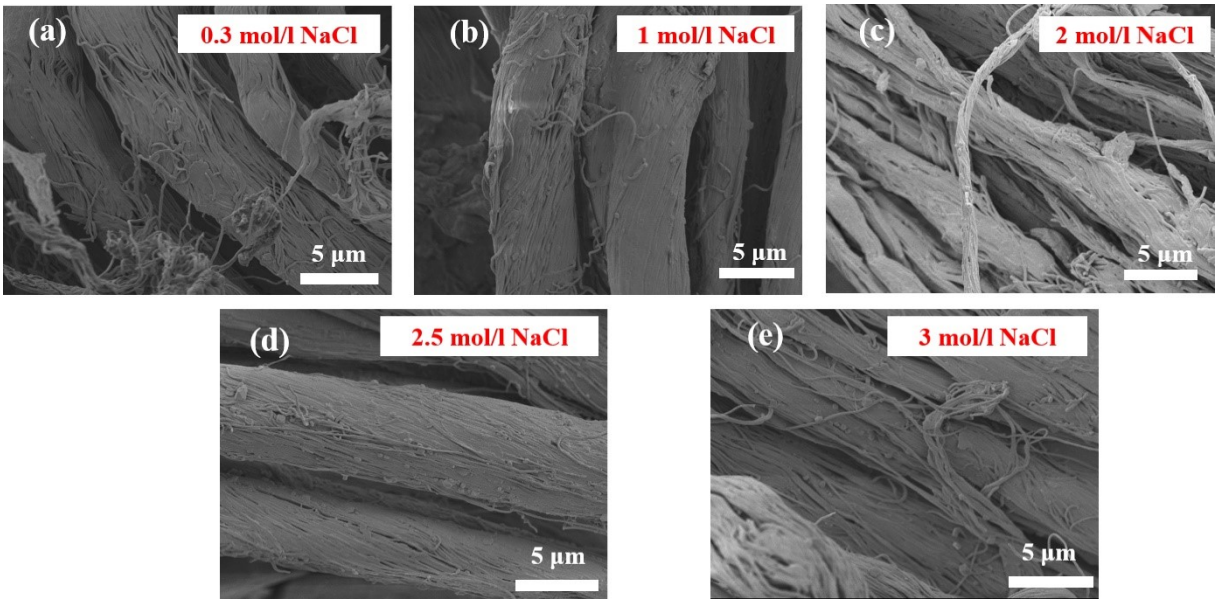

Fig. S7. Cross-sectional SEM images of (a–e) leather soaked in 0.3 mol/L, 1 mol/L, 2 mol/L, 2.5 mol/L, and 3 mol/L NaCl solutions, respectively.

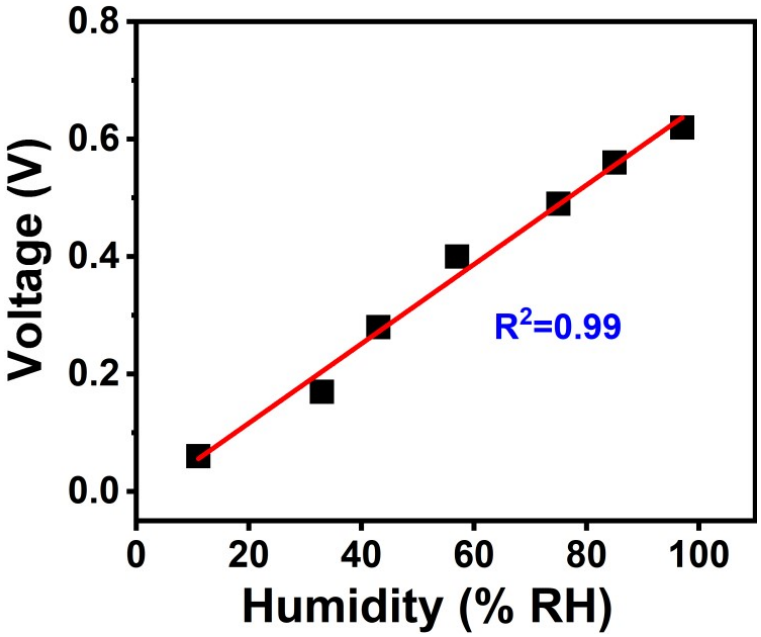

Fig. S8. Linear response relationship of the voltage and humidity (0.3 mol/L NaCl).

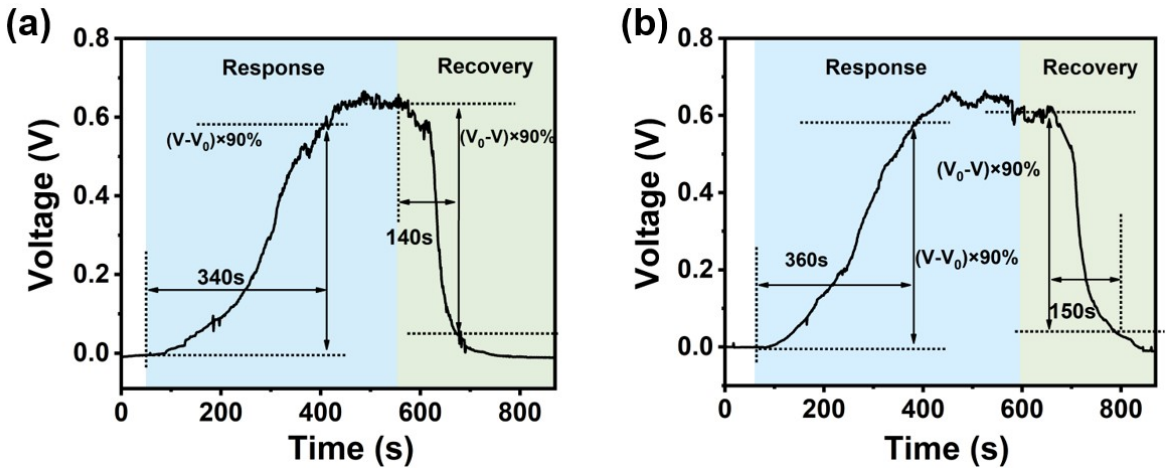

Fig. S9. The voltage with time for a single absorption and desorption cycle of the sensor. (a) The response time and recovery time for the first cycle are 340 s and 140 s, (b) the response time and recovery time for the second cycle are 360 s and 150 s.

The response time is calculated as the time required from the initial voltage to respond to 90% of the voltage in the final steady state. The recovery time is calculated as the time required from the initial voltage to the response to the final return to 90% of the voltage in the steady state.

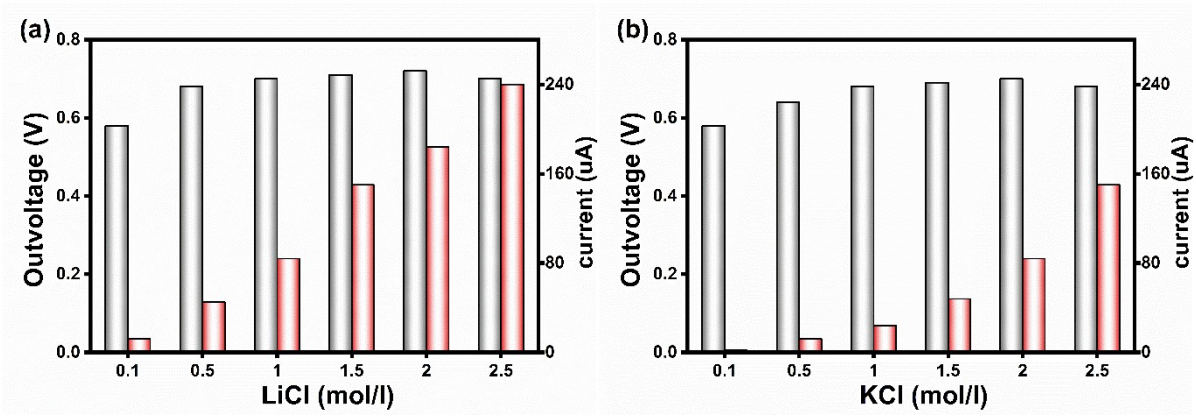

Figure S10. Output performance of LECH sensors with KCl and LiCl electrolytes. Maximum voltage and short-circuit current as a function of salt concentration for devices using **(a)** KCl and **(b)** LiCl as the hygroscopic electrolyte. All measurements were conducted under 97% relative humidity (RH). The data demonstrate the universal concentration-dependent trend and the tunable output based on ion species.

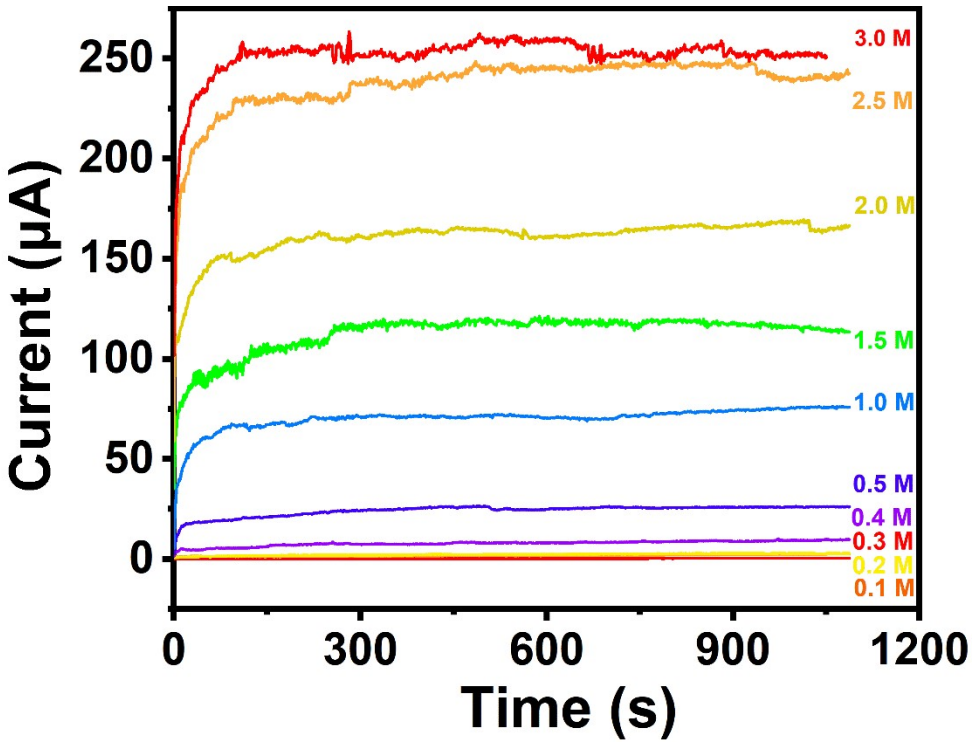

Fig. S11. Test curves of output current for sensors soaked in different concentrations of NaCl (0.1, 0.2, 0.3, 0.4, 0.5, 1.0, 1.5, 2.0, 2.5, 3.0 mol/L) at 97% RH.

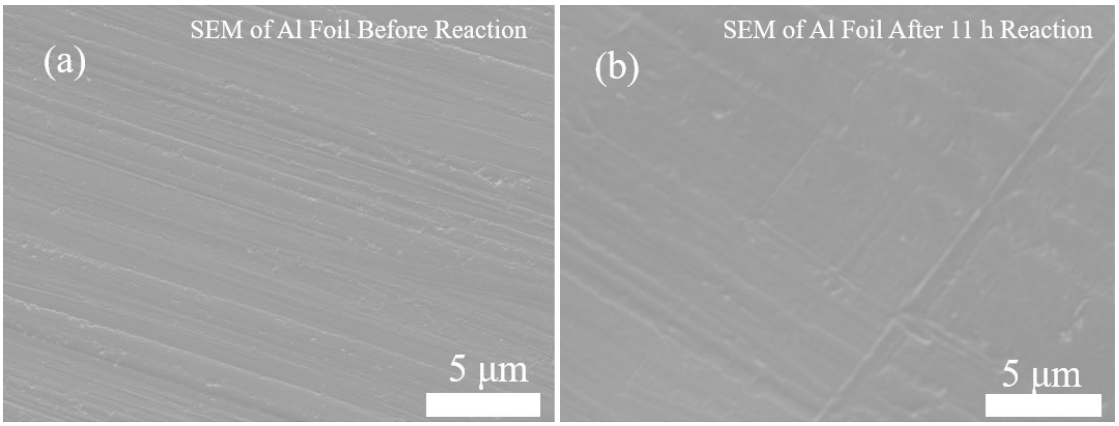

Fig. S12. SEM images of the Al electrode (a) before and (b) after 11 h operation at 97% RH, showing no obvious corrosion or surface damage.

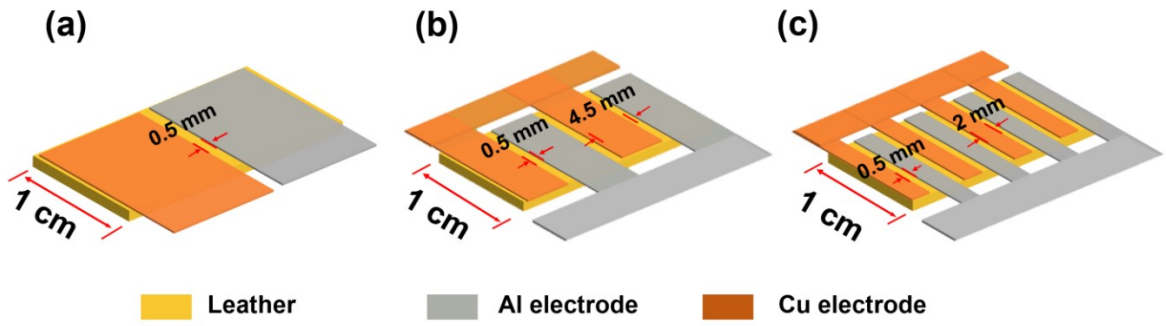

Fig. S13. Schematic diagram of the device with a different number of electrodes. (a) one pair, (b) two pairs, (c) four pairs, respectively

Attention: The size of the device remains at 1 × 2 cm^2, and the distance between the Cu and Al electrodes remains at 0.5 mm.

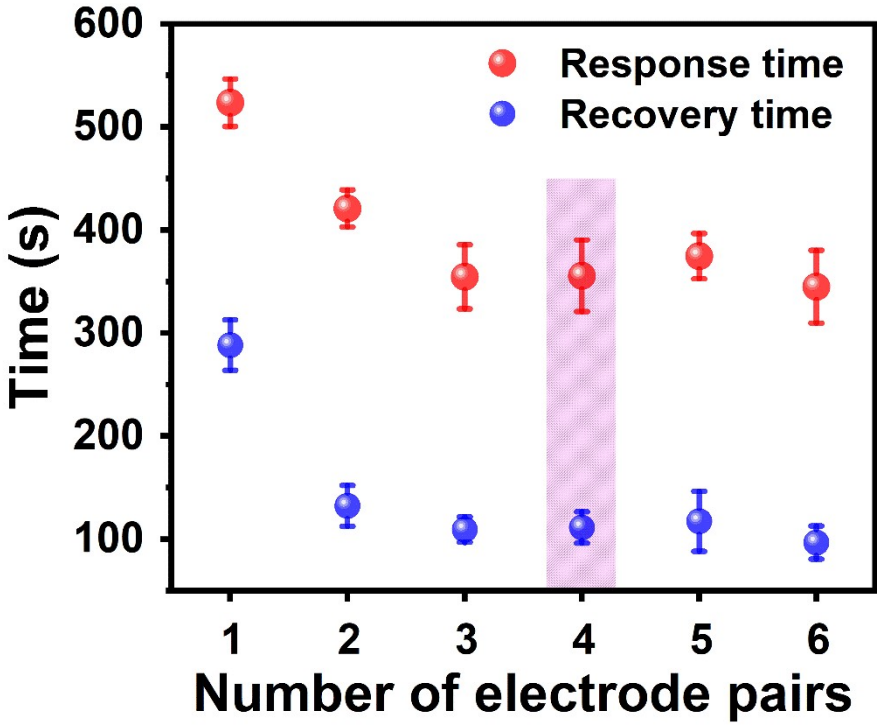

Fig. S14. LECH devices voltage with different numbers of electrodes pairs (1, 2, 3, 4, 5, and 6). Test conditions were 97% RH and 25℃. Data are mean ± standard deviation (n = 3 independent experiments).

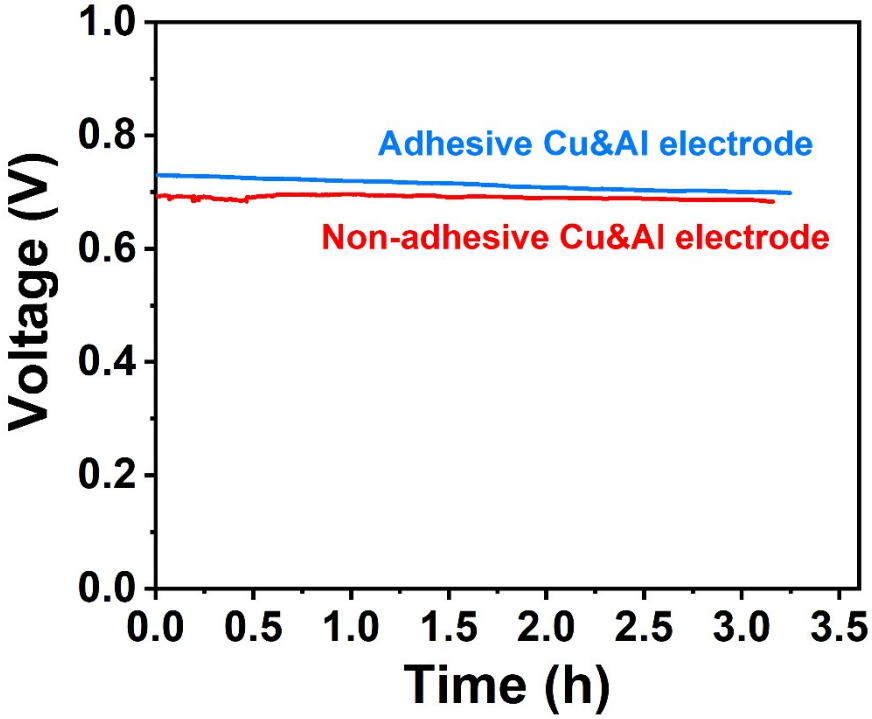

Fig. S15. The output voltage for sensor with adhesive and non-adhesive electrodes.

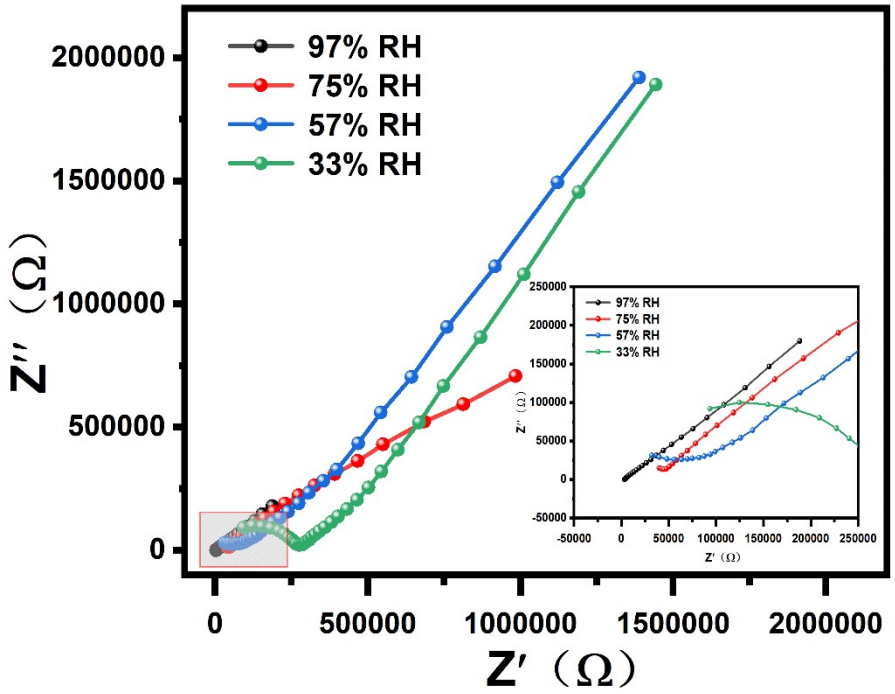

Fig. S16. Nyquist plots of the LECH sensor at different RH, showing reduced resistance with increasing humidity.

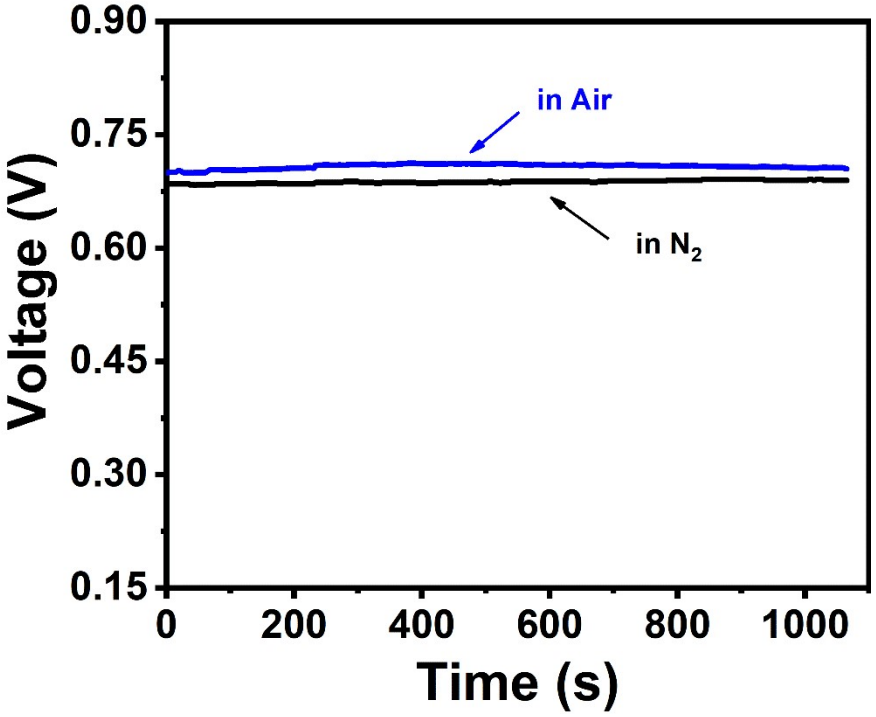

Fig. S17. Output voltage curve of the LECH in air and pure N_2.

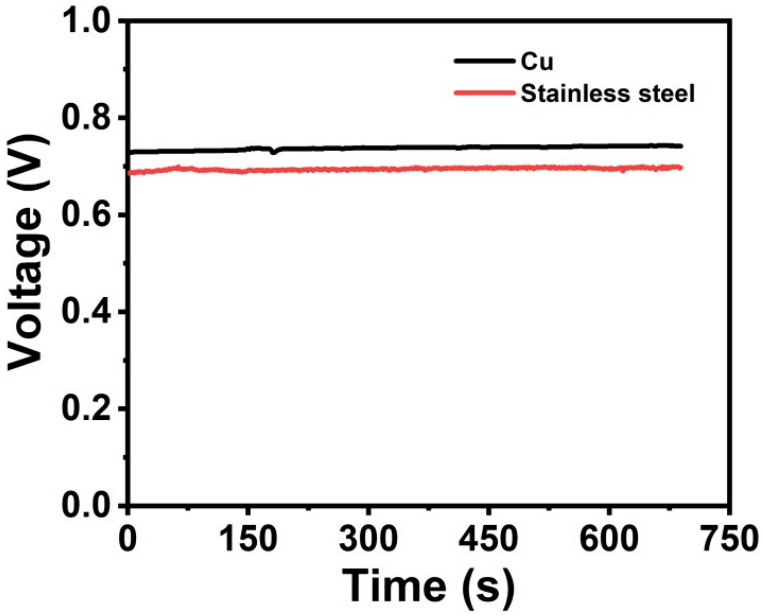

Fig. S18. The Output voltage curve of devices by using copper electrode and stainless steel electrode as device electrode respectively.

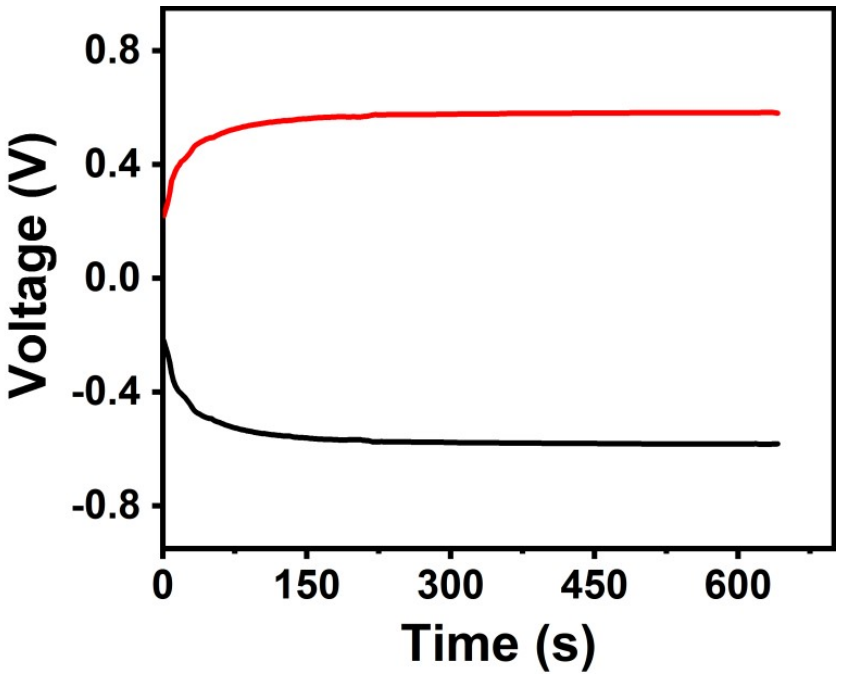

Fig. S19. Response curves of the LECH at positive and negative connections.

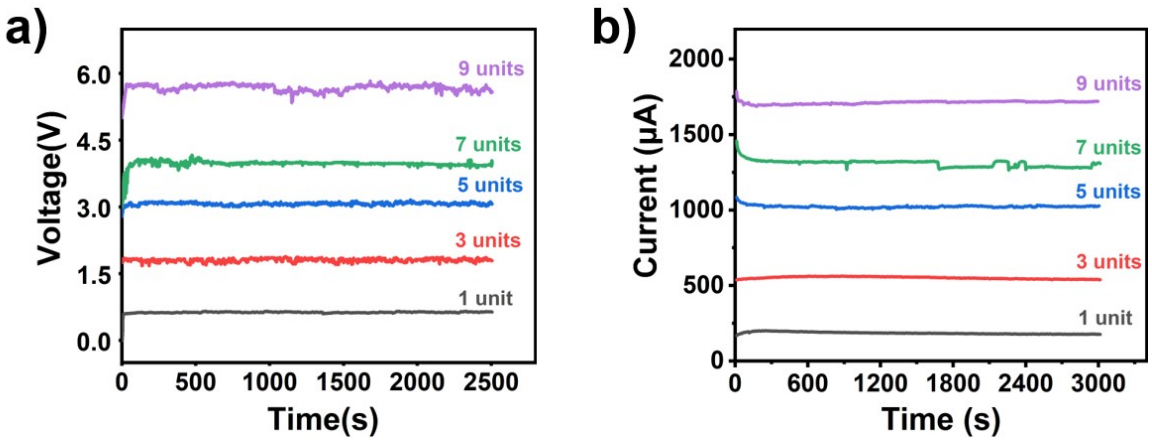

Fig. S20. Variation for 1–9 units LECH devices single components. (a) Output voltage connected in series, (b) Output current connected in parallel.

Table S1. Content of NaCl in unit leather (mg/cm^2)

NaCl (mol/L)	Dry leather (mg)	Dry NaCl/leather (mg)	Loading amount of NaCl (mg)	Loading amount of NaCl in the unit leather (mg/cm^2)
0.1	116.3	116.5	0.2	0.1
0.2	111.2	112.5	1.3	0.65
0.3	114.1	116.8	2.8	1.4
0.4	113.4	116.7	4.1	2.05
0.5	110.8	119.2	5.4	2.7
1	118.9	129.4	9.8	4.9
1.5	116.6	132.2	15.1	7.55
2	116	134.4	18.4	9.2
2.5	115.6	140.1	23.1	11.55
3	112.4	138.8	25.7	12.85

Method: Cut 10 pieces of leather with an area of 2 cm^2 (1 cm × 2 cm), weighing the mass of each piece of dry leather (m_1), 10 pieces of leather were soaked in different concentrations of NaCl solution for 10 min. Remove the leather, put it in the oven at 50℃ to dry for 8 h, and weigh each piece of dry NaCl/leather (m_2). The loading amount of NaCl in a unit of leather is calculated as the formula : $(m_2–m_1)/2$.

Table S2. Comparison of the power generation of the LECH sensor and other reported ion diffusion and electrochemical power generation humidity sensors.

Materials	Detetecting range (RH)	Maximum Voc (V)	Power (μW)/ Isc (μA)	Device type	Ref
PSSA/PDDA	20−100%	1.1	~2.6/22.7	ion diffusion	1
Bilayer of polyelectrolyte film	25−85%	1.38	5.52/4	ion diffusion	2
pNIPAm	68.5−82.9%	1.86	10.14/21.8	ion diffusion	3
Carbon-black-coated cotton fabric	20−85%	0.53	0.256/3.91	ion diffusion	4
Ni–Al LDH films	56−80%	0.6	0.045/0.3	ion diffusion	5
GO	20−90%	0.77	~0.25/~1.3	electrochemistry	6
GO/SF/LiBr	11.3−84.3%	1.29	~12.9/~40	electrochemistry	7
NF/GO	36.4−97%	0.83	~0.45/~2.2	electrochemistry	8
LiCl	10.9−91.5%	0.55	0.29/2.14	electrochemistry	9
NaCl/OH-MWCNTs	20.52/62	1.32	20.52/62	electrochemistry	10
Nb2CTx/HA	10.9−91.5%	0.7	0.96/~7.4	electrochemistry	11
NaCl/sodium alginate	10.9−91.5%	0.7	2.63/24	electrochemistry	12
NaCl	41.1−91.5%	0.58	1.33/7.9	electrochemistry	13
Nacl/Leather	10.9−91.5%	0.75	8.79/250	electrochemistry	This work

1 T. He, H. Wang, B. Lu, T. Guang, C. Yang, Y. Huang, H. Cheng, L. Qu, Fully printed planar moisture-enabled electric generator arrays for scalable function integration, *Joule.,* 2023, **7**, 935–951.

2 H. Wang, Y. Sun, T. He, Y. Huang, H. Cheng, C. Li, D. Xie, P. Yang, Y. Zhang, L. Qu, Bilayer of polyelectrolyte films for spontaneous power generation in air up to an integrated 1,000 V output, *Nat. Nanotechnol*., 2021, **16**, 811–819.

3 C. Liu, S. Wang, X. Wang, J. Mao, Y. Chen, N. Fang, S. Feng, Hydrovoltaic energy harvesting from moisture flow using an ionic polymer-hydrogel-carbon composite, *Energy Environ. Sci*., 2022, **15**, 2489–2498.

4 T. Yun, J. Bae, A. Rothschild, I. Kim, Transpiration Driven Electrokinetic Power Generator, *ACS Nano.,* 2019, **13**, 12703−12709.

5 J. Tian, Y. Zang, J. Sun, J. Qu, F. Gao, G. Liang, Surface charge density-dependent performance of Ni-Al layered double hydroxide-based flexible self-powered generators driven by natural water evaporation, *Nano Energy*., 2020, **70**, 104502.

6 D. Lei, Q. Zhang, N. Liu, T. Su, L. Wang, Z. Ren, Z. Zhang, J. Su, Y. Gao, Self-Powered Graphene Oxide Humidity Sensor Based on Potentiometric Humidity Transduction Mechanism, *Adv. Funct. Mater*., 2022, **32**, 2107330.

7 S. Li, Y. Zhang, X. P. Liang, H. M. Wang, H. J. Lu, M. J. Zhu, H. M. Wang, M. C. Zhang, X. P. Qiu, Y. F. Song, Y. Y. Zhang. Humidity-Sensitive Chemoelectric Flexible Sensors Based On Metal-Air Redox Reaction For Health Management, *Nat Commun*., 2022, **13**, 5416.

8 W. Lu, Q. Zhang, N. Liu, D. Lei, Z. Ren, J. Yin, P. Jia, Y. Gao, Nylon Fabric/GO Based Self-Powered Humidity Sensor Based on the Galvanic Cell Principle with High Air Permeability and Rapid-Response, *Small*., 2024, **20**, 202306463.

9 Q. Zhao, Z. Duan, Y. Wu, B. Liu, Z. Yuan, Y. Jiang, H. Tai, Facile primary battery-based humidity sensor for multifunctional application, *Sens. Actuators B: Chem*., 2022, **370**, 132369.

10 M. Zhang, Z. Duan, B. Zhang, Z. Yuan, Q. Zhao, Y. Jiang, H. Tai, Electrochemical humidity sensor enabled self-powered wireless humidity detection system, *Nano Energy.,* 2023, **115**, 108745.

11 Q. Zhao, Y. Jiang, L. Yuan, Z. Yuan, B. Zhang, B. Liu, M. Zhang, Q. Huang, Z. Duan, H. Tai, Hydrophilic hyaluronic acid-induced crumpling of Nb2CTx nanosheets: Enabling fast humidity sensing based on primary battery, Sens. Sens. Actuators B: Chem., 2023, **392**, 134082.

12 Z. Duan, B. Zhang, M. Zhang, Z. Yuan, Y. Jiang, H. Tai, High-performance electrochemical power generation humidity sensor based on NaCl/sodium alginate humidity sensing electrolyte and Cu/Zn electrodes for visual humidity indication and respiratory patterns detection, *Sens. Actuators B: Chem*. 2024, **409**, 135585

13 Z. Duan, Z. Yuan, Y. Jiang, Q. Zhao, Q. Huang, Y. Zhang, B. Liu, H. Tai, Power generation humidity sensor based on primary battery structure, *Chem. Eng. J*., 2022, **446**, 136910.